Climate **2013**, *1*, 120-147; doi:10.3390/cli1030120

OPEN ACCESS

climate

ISSN 2225-1154

www.mdpi.com/journal/climate

Article

Exploring Aerosol Effects on Rainfall for Brisbane, Australia

Michael Hewson [1,2,*], Hamish McGowan [1], Stuart Phinn [2], Steven Peckham [3] and Georg Grell [3]

[1] Climate Research Group, The School of Geography, Planning and Environmental Management, The University of Queensland, Brisbane Queensland 4072, Australia; E-Mail: h.mcgowan@uq.edu.au

[2] Biophysical Remote Sensing Group, The School of Geography, Planning and Environmental Management, The University of Queensland, Brisbane Queensland 4072, Australia; E-Mail: s.phinn@uq.edu.au

[3] Earth Systems Research Laboratory, National Oceanic and Atmospheric Administration, Boulder, CO 80305-3337, USA; E-Mails: steven.peckham@noaa.gov (S.P.); georg.a.grell@noaa.gov (G.G.)

***** Author to whom correspondence should be addressed; E-Mail: m.hewson@uq.edu.au; Tel.: +61-7-334-67023.

Received: 23 April 2013; in revised form: 30 July 2013 / Accepted: 7 October 2013 / Published: 28 October 2013

Abstract: The majority of studies assessing aerosol effects on rainfall use coarse spatial scale (1° latitude/longitude or more) and multi-seasonal or decadal data sets. Here, we present results from a spatial correlation of aerosol size distribution and rain rate for selected stratiform and cumuliform precipitation events. The chemistry transport version of the Weather Research and Forecasting model was used to estimate aerosol parameters during rain events Aerosol maps were then compared with observations of rainfall using geostatistics for the first time. The cross-variogram analysis showed that anthropogenic aerosol was associated with areas of less intense rain within the stratiform system studied. For cumuliform systems, cross-variogram analysis found that anthropogenic emissions may be associated with enhanced rain downwind of aerosol emissions. We conclude that geostatistics provides a promising new technique to investigate relationships between aerosols and rainfall at spatial scales of 1 km which complements more commonly used methods to study aerosol effects on rainfall.

Keywords: natural and anthropogenic emission; spatial analysis; geostatistics

1. Introduction

1.1. Aerosol Effects on Rainfall and the Primary Study Objective

The existence of the hydrological cycle, weather systems and climate is in part, due to the presence of particles suspended in the atmosphere capable of allowing cloud droplets to form [1]. Aerosols, essential to rain generation, include natural particles; dust, sea salt and, biogenic emissions for example, as well as direct or fugitive emissions from anthropogenic activities including disturbance of soil, biomass burning, and residential, transport and industrial emissions to air. In their Fourth Assessment Report, the Intergovernmental Panel on Climate Change noted that the size distribution of aerosols is critical to atmospheric processes that influence the climate including aerosol effects related to the scattering and absorption of energy and aerosol effects on cloud droplet size and concentration [2]. Aerosol and its effect on rainfall has been the subject of discussion for some 50 years [3]; for example, one of the indirect effects of aerosol is that rain may be suppressed in warm phase clouds by anthropogenic particles [4].

Comparing Australian rainfall records for a 50 year period, Warner [5] concluded that carbonaceous aerosol from sugar cane farm fires increased the concentration and reduced the size of cloud droplets thereby inhibiting rainfall. Rosenfeld [6] presented satellite images classified for cloud droplet size; one of them for an expanse of cloud in which droplets were generally coalescing into rain exhibited elongated plumes of smaller cloud droplets downwind of pollution sources in South Australia. This suggested that cloud droplet growth was inhibited in polluted clouds thereby suppressing precipitation. Motivating our study, Bigg [7] examined the spatial distribution of rainfall datasets (1970–2004) around the city of Brisbane, Australia and concluded that a possible aerosol effect on rainfall should be further examined.

Many recent studies of aerosol effects on cloud droplet size and precipitation have used data sets of seasonal or annual temporal scale and spatial scales in the order of 1 degree latitude/longitude or larger. Using four years of remotely sensed monthly mean aerosol optical thickness and precipitation observations for Houston and New York, Jin *et al*. [8] found no clear relationship between monthly mean aerosol optical thickness and rainfall. Comparing rain radar intensity with three fine mode particulate ($PM_{2.5}$) monitors in Atlanta, Lacke *et al*. [9] cited inconclusive results: on high aerosol load days, $PM_{2.5}$ was associated with higher rain rates. On low aerosol load days, $PM_{2.5}$ was associated with lower rain rates. Koren *et al*. [10] found a positive correlation between aerosol abundance and rain rate comparing four different aerosol regimes in 10 degree square regions using data at 1 degree resolution. For St Louis USA using a cloud-resolving meso-scale model, van den Heever and Cotton [11] found that once convection processes were evident, the addition of anthropogenic aerosol resulted in cloud water and precipitation forming earlier downwind of the urban centre than that for model control runs. The authors further demonstrated that the modelled rain response was weaker for higher levels of background aerosol indicating that the relative concentrations of natural and anthropogenic aerosol is important to the extent to which aerosol effects are observed. Using monthly averaged model output, Yang *et al*. [12] compared clean and polluted regions of Californian coastal marine stratocumulus clouds and found that increased anthropogenic aerosol reduced precipitation. The authors also noted that the extent of aerosol effects was determined by the relative concentration

of oceanic natural aerosol emissions. Using the ECHAM5 general circulation model on a global scale, Lohman [13] concluded that increased greenhouse gas and anthropogenic aerosol emissions was geographically distributed with increased convective system precipitation. On the other-hand, Han *et al*. [14] using an idealised weather model with a horizontal domain of 256 km, found that rainfall can be delayed in deep cumuliform systems 20 km downwind of the city. At decadal temporal scales, Lin [15] found that regions in China with decreasing pollution had increased rainfall frequency while Zhang *et al*. [16] found that during the summer monsoon, clean air from the Southern Hemisphere diluted aerosol concentrations in eastern China and that increasing rainfall frequency reduced pollution concentration. While some consensus on the effects of aerosols on cloud microphysical processes is evident in the literature, researchers point to the need to study the aerosol effects on rainfall at less aggregated spatial and temporal scales.

Andreae and Rosenfeld [4] in their review of research examining anthropogenic aerosol effect on rain summarised the process for shallow, short-lived, warm phase clouds as follows: in air with elevated concentrations of smaller anthropogenic aerosols, the clouds that form contain higher concentrations of smaller droplets reduce the formation of warm phase cloud rain by decreasing the collision coalescence process. They also concluded that deep convective rainfall was enhanced because aerosols not activated at lower levels in the warm phase of the cloud are transported aloft, where they may become efficient ice nuclei.

To date most aerosol effect studies have used either remotely sensed atmospheric properties aggregated over spatial and temporal scales or global climate models over multiple years. Our primary objective was to geospatially compare aerosol size distribution with rain rate for three rain events with data at spatial and temporal scales sufficient to resolve the interactions between these parameters for the subtropical city of Brisbane, Australia. Accordingly, our research complements the current literature concerning aerosol effects on rainfall by contributing a geographical analysis through a case study approach.

1.2. Potential Confounding Processes and Secondary Study Objectives

Relationships between aerosol, clouds and rainfall are subject to a range of associated atmospheric properties, principal among them: atmospheric stability [8,17], water vapor content [18,19], and boundary layer depth [8]. Authors of recent aerosol indirect effect studies acknowledged that the certainty of their results is made difficult by the complex nature of cloud microphysics and dynamics as well as complicated relationships between atmospheric parameters. In a study comparing nitrous-dioxide with rainfall for China, Lin *et al*. [20] found that gas phase anthropogenic emissions and precursors to secondary aerosol reduced the frequency of rainfall, noting that the relationship between pollution and rainfall can be masked by cloud dynamics. In disputing Rosenfeld's [6] conclusion that pollution could have produced the satellite observed downwind regions of reduced cloud droplet size in otherwise homogenous water phase clouds, Ayers [21] commented that cloud dynamics rather than cloud microphysics could explain the observed decreased cloud droplet sizes. Ayers [22] notes that measurements of water vapor content and air-mass stability were needed to explain aerosol and cloud interaction.

Our secondary objective was to explore the effect of anthropogenic aerosol on rainfall; where possible, isolating the data for atmospheric parameters and dynamic processes that could counter explain the results of the present study's primary objective. We present geospatial comparisons of aerosol size distribution with rain rate stratified for cloud water content and vertical air movement representing cloud dynamics and atmospheric stability. Further, we spatially analysed rain rate with terrain height, Earth skin temperature and wind fields representing orographic lifting, urban enhanced convection and low level wind convergence, respectively.

2. Materials and Methods

2.1. Study Area

The study area (Figure 1), centred at 153°E and 27°S, is the city of Brisbane situated on the east coast of Australia—home to some 2.2 million people in the greater urban area.

Figure 1. The study area extent centred on the sub-tropical city of Brisbane, Australia. Satellite image provided by Geosciences Australia.

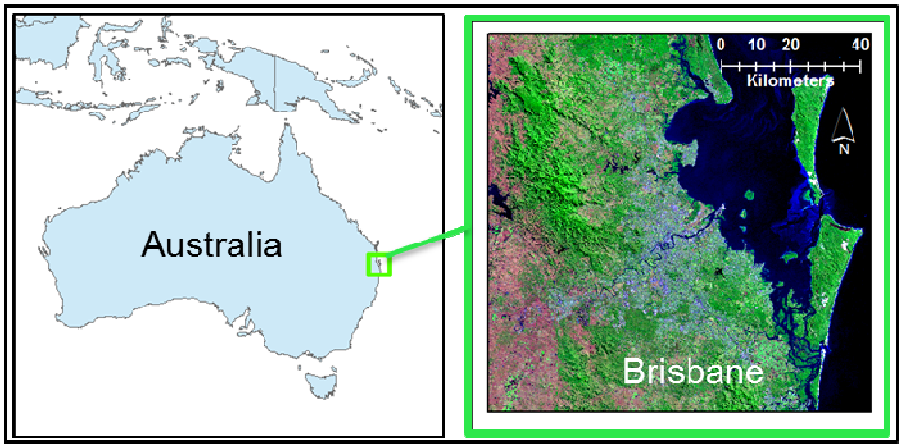

Although aerosol loads across Australia are generally low by global standards [23], Chan's [24] Brisbane aerosol inventory apportioned sources of fine particulate by mass as: 24% elemental carbon; 21% secondary organics; 15% biomass burning; 14% secondary sulphate; and 6% direct contribution by vehicle exhausts. The majority of the fine mode aerosol fraction in Brisbane was found to have an anthropogenic source. Cheung *et al*. [25] later confirmed that the major pollution sources were transport and industrial emissions.

2.2. Data—Rain Events and Rain Rate

Three rain events in the years 2009–2012 were selected for study to contrast cumuliform and stratiform rainfall close to anthropogenic aerosol emission sources (Brisbane, Australia) during satellite overpass times.

Event 1—on Wednesday afternoon, December 2, 2009, an inland trough west of Brisbane separated moist air to the east from dry inland air (Figure 2). Westerly winds aloft directed rain showers from the west toward the city. A satellite image from the Moderate Resolution Imaging Spectroradiometer

(MODIS); at 03:40 UTC (2:40 pm local time) indicated cumuliform cloud under an optically thin, higher stratus layer. The MODIS cloud top pressure image values were around 490 hPa for the cumuliform layer indicating most likely mixed phase stratocumulus (Sc) cloud. The 03:30 UTC Brisbane airport meteorological area report (METAR), revealed a cloud regime of: 1 okta of stratus (St) at a cloud base of 450 m above mean sea level; 4 oktas of Sc at 900 m and 7 oktas of Sc at 1,700 m. A ceilometer located in the centre of Brisbane, at the University of Queensland (UQ), showed rainfall from a cloud base at 1,100 m. (we add comma for numbers over 1000, just for your reference)

Figure 2. Mean sea level pressure (MSLP) chart for 06:00 UTC and MODIS band 1 image 03:40 UTC December 2, 2009 (We set the date as 2 December 2009, just for reference).

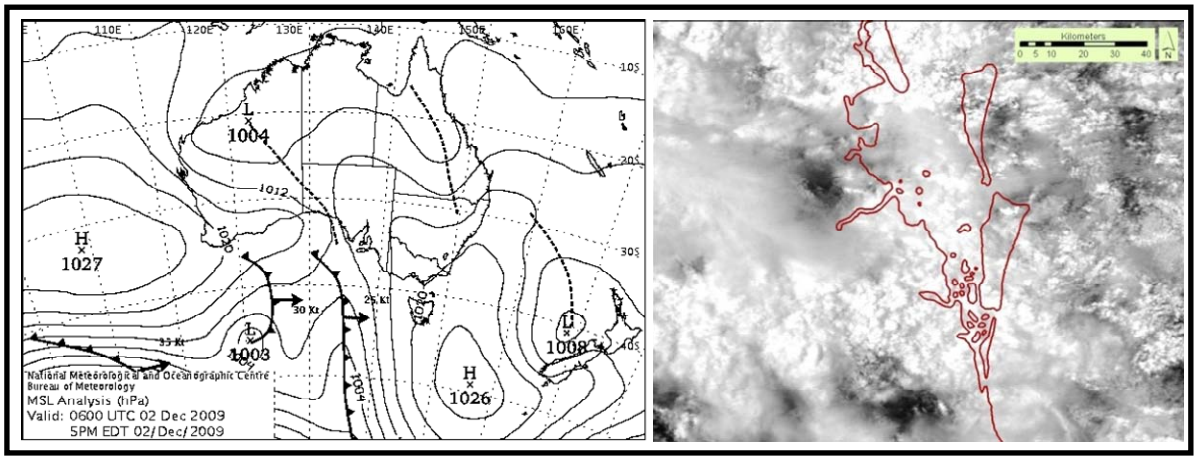

Event 2—on Saturday, September 25, 2010, a surface trough extended across inland Queensland directing a humid and unstable air mass over Brisbane (Figure 3). The 03:40 UTC MODIS image shows cumuliform cloud types under a substantially higher, optically thin, stratus layer. The UQ ceilometer indicated scattered rainfall from cloud bases between 1 and 2 km. The 03:30 UTC METAR reported a weather regime of mixed cloud types: 1 okta of cumulus cloud (Cu) at 820 m; 6 oktas of Sc at 1,680 m; and 8 oktas of altostratus (As) cloud at 6,100 m.

Figure 3. MSLP chart for 06:00, MODIS band 1 image 03:40 UTC, September 25, 2010.

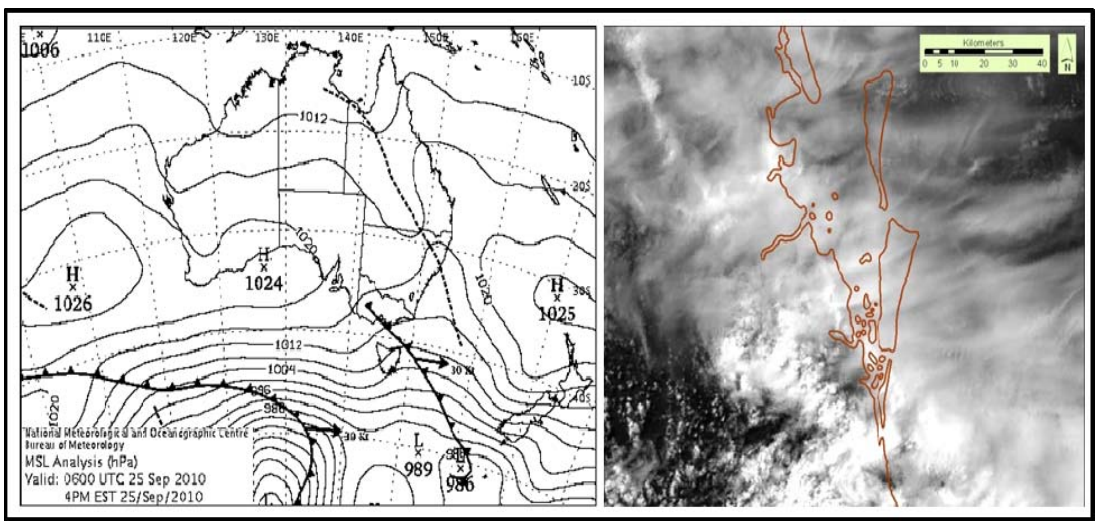

Event 3—on Thursday, November 24, 2011, Brisbane experienced light rain to mid-morning. A weak ridge maintained a moist onshore wind over the east coast before a coastal trough and associated southerly wind change moved slowly north (Figure 4). The 23:15 UTC (10:15 am local time) MODIS image indicated stratiform cloud cover and the UQ ceilometer indicated rain from a cloud base at around 500 m. The 23:00 UTC METAR reported: 1 okta of St at 180 m; and 6 oktas of St at 460 m.

Figure 4. MSLP chart for 00:00 UTC 24 November 2011 and MODIS band 1 image 23:15 UTC 23 November 2011.

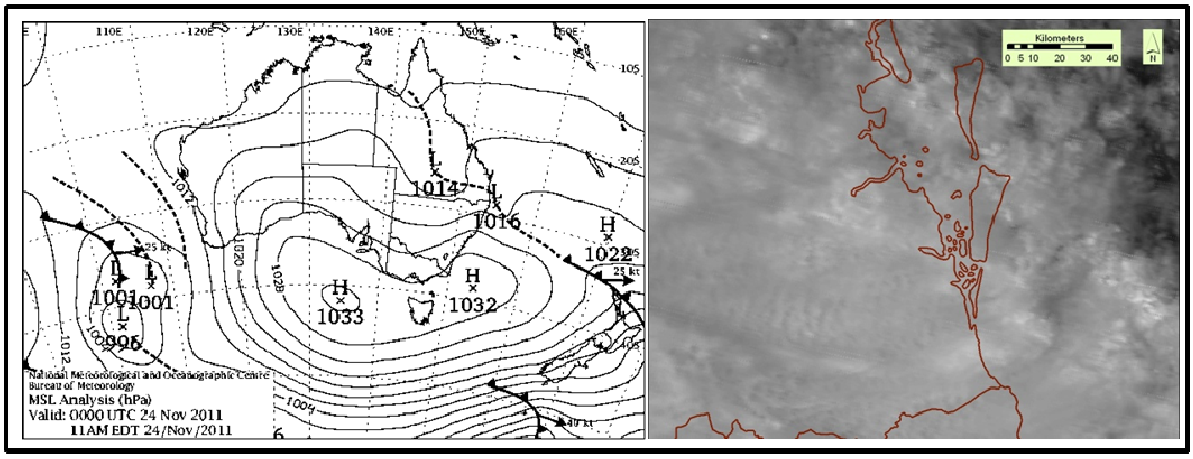

For the remainder of this paper the three rain events were named: (1) Sc2009 for December 2, 2009; (2) Cu/Sc2010 for September 25, 2010; and (3) St2011 for November 24, 2011.

The Australian Government Bureau of Meteorology (BoM) provided geographic information system ready images of rain intensity from their Mt. Staplyton Doppler rain radar site located 33 km south-east of Brisbane's city centre. The dimensionless rain rate given as integer values are processed from radar reflectivity echoes of water droplet size hydrometeors at 6 min intervals. The rain rate images are composed of polygons that within 60 km from Mt. Stapylton are 1 km or less in width.

2.3. Geostatistics

Atmospheric parameters are distributed in space and time and a statistic is needed to provide some quantitative measure of their spatial correlation. Geostatistics is a set of statistical tools that incorporates the spatial dimension to co-varying parameter comparisons [26]. Here, we use geostatistics graphs such as the semi-variogram which display the degree of spatial autocorrelation at increasing distance for individual variables. The cross-variogram shows the degree of joint variability of two parameters at increasing distance. The data points on the graph are collectively called the "experimental variogram". The features of variography used to interpret the spatial auto/cross-correlation of parameters include: (1) the range—the approximate lag distance between sample points at which the spatial auto-correlation of the variable is first minimized; (2) the sill—the semi-variance value where spatial autocorrelation no longer exists at the experimental variogram range; and (3) the nugget—the semi-variance value at the shortest lag distance between sample points representative of measurement error. If parameter values are similar to each other at a given distance they will have a smaller semi-variance value in the variogram. The focus of spatial analysis was to interpret experimental

cross-variograms to identify the level of spatial correlation between jointly varying atmospheric variables—rainfall and aerosol—considering controlling environmental factors.

Since geostatistics is based on stochastic processes, non-Gaussian data sets should be transformed if possible [27]. Atmospheric data, particularly rain-rate [28], often exhibit non-Gaussian data distribution or non-stationarity trends; that is, the mean of the data set varies within a defined areal extent. Trend violates second order stationarity and needs to be treated before the calculation of an experimental variogram [29]. Logarithmic transformations were used to reduce the generally skewed data distributions of the present study. Cross-variograms computed for an anisotropic direction perpendicular to the trend was another recommended way of ameliorating the trend in the data [27]. Universal co-kriging (kriging-with-drift for two variables) cross-variograms were calculated in the "R" open source spatial statistics software package "Gstat" [30] since this class of geostatistics was shown to deal with the drift in rainfall data to some extent [31]. To our knowledge, geostatistics has not yet been used to analyse the aerosol effects on rainfall.

Discussing the scale of data used in studies that quantify aerosol effects on cloud, McComiskey and Feingold [32] noted that up-scaling and aggregating atmospheric quantities causes biases and error in statistical inferences because of the smoothing effects of the aggregation. It has long been understood that scale aggregation by averaging has a deleterious effect on statistical calculations [32] and accordingly, we follow the authors' advice to use 1 km spatial resolution as an appropriate scale for characterising aerosol-cloud processes from model and satellite remote sensed atmospheric parameters.

2.4. Selection of an Aerosol Parameter

Following Yu *et al*. [33], aerosol size distribution was characterized by the dimensionless Angstrom wavelength exponent represented by the symbol α in the present paper. Examining aircraft-measured aerosol vertical variability, Sheridan *et al*. [34] found that α, unlike aerosol concentration, is relatively constant through the mixed layer, making α a suitable proxy for the column integrated aerosol size distribution. Higher α value represents smaller aerosol sizes while smaller α value indicates that coarse mode aerosol dominates the size distribution. Chin *et al*. [35] advise that α values of:

- less than 1 indicates that coarse mode aerosol predominate (0.2–0.5 are dust aerosol);
- 1–1.8 indicates fine mode particles of many species; and
- greater than 2 indicates that fine mode anthropogenic aerosol dominate the air column.

Dusek *et al*. [36] showed that aerosol size distribution alone can explain the variability in cloud drop nucleating activity which makes it easier to quantify the effects of aerosols on clouds rather than trying to measure atmospheric particle chemistry [37]. Further, given that over a 3 h period most aerosol gains a level of hygroscopicity such that virtually any aerosol of the right size can potentially become cloud condensation nuclei [4], aerosol size distribution was chosen as the key aerosol parameter to correlate with rainfall.

2.5. Data—WRF-Chem Aerosol

Optically based satellite remote sensing of aerosol during rain events was not possible since the instruments do not see through clouds. Lidar remote sensing of aerosol through cloud was possible but

only for a narrow swath width, unsuitable for the present study. Accordingly, aerosol optical depth (AOD) maps, from which α was calculated, were provided by the online coupled, chemistry transport version of the numerical Weather Research and Forecasting model (WRF-Chem) further described by Grell *et al*. [38].

Configuring WRF-Chem involved critical selections of physics, aerosol transport and gas-phase chemistry schemes. We compared eight common WRF-Chem scheme combinations with MODIS satellite aerosol parameters (AOD and α) [39] in clear sky conditions to select an optimum model configuration. The sampling scheme for the trial was located over an area of ocean off the coast near the city of Brisbane because MODIS derived aerosol images over land surfaces, particularly higher albedo surfaces, have been subject to a known persistent bias [40]. Sampling points were placed further than 15 km from cloud because MODIS AOD measurements can be spuriously biased high from the influence of radiation scattering from nearby clouds or cloud droplets being misidentified as aerosol [41–43]. The results indicated that 600 nm α from the WRF-Chem "Carbon Bond Mechanism—Zaveri" gas-phase chemistry and "Model for Simulating Aerosol Interactions and Chemistry" (MOSAIC) 4 bin aerosol transport scheme combination were strongly correlated with MODIS 550 nm α, $\rho = 0.61$. However, due to resource limitations of the host research computing centre, a less computationally expensive WRF-Chem MADE-SORGAM (Modal Aerosol Dynamics Model for Europe—Secondary Organic Aerosol Model) modal aerosol transport scheme coupled with the RADM2 (Regional Acid Deposition Model version 2) [44] gas phase chemistry scheme was chosen for the present study. In this configuration, 600 nm α was moderately correlated with MODIS 550 nm α, $\rho = 0.45$ and 300 nm α with a stronger correlation at $\rho = 0.58$. MADE divides aerosol mass into three size distribution sections depending on a look up table that assigns the modes (Aiken, accumulation and coarse mode) [45]. Wu *et al*. [46] noted that maps of WRF-Chem MADE-SORGAM eight-day averaged AOD intensity gradients compared well on a visual inspection with MODIS eight-day averaged areal AOD images. In the context of an aerosol modeling test-bed, Fast *et al*. [47] concluded that MADE-SORGAM performed as well as a more advanced 8 bin MOSAIC sectional aerosol parameterization while being computationally cheaper.

WRF-Chem version 3.3.1 was configured with 2 domains at a ratio of 1:3. The nested inner domain, from which the model aerosol output is drawn, was a square area of 200 grid points at a spatial resolution of 1 km to ensure α was calculated at the same scale as rain-rate. The WRF-Chem meteorological boundary conditions were updated by six hourly weather observations made available by the US National Centre for Environmental Prediction and idealized chemistry lateral boundary conditions were used as described by Peckham *et al*. [48]. WRF-Chem physics scheme choices were informed by a number of WRF-Chem aerosol studies [49–53] as follows:

- Lin microphysics scheme
- Rapid Radiative Transfer Model for Global Climate Models short-wave and long-wave radiation schemes;
- Yonsei University planetary boundary layer scheme;
- Monin-Obukhov surface layer scheme; and
- Unified Noah land surface scheme.

WRF-Chem aerosol emissions were obtained from global databases:

- as at 2000, Reanalysis of the Troposphere (RETRO) anthropogenic chemical emissions [54] at 0.5 degree resolution;
- as at 2006, Goddard Chemistry Aerosol Radiation and Transport (GOCART) anthropogenic and background emissions [35] at 1 degree resolution;
- as at 2005, Emissions Database for Global Atmospheric Research (EDGAR) global anthropogenic emissions [55] at 0.1 degree resolution; and
- as at 2003, Model of Emissions of Gases and Aerosols from Nature (MEGAN) biogenic aerosol emissions [56] at 1 km resolution.

We found that all WRF-Chem aerosol transport schemes skewed α to fine mode aerosol when compared with measured α from the NASA AERONET sunphotometer located at UQ. This is most likely due to the coarse resolution of WRF-Chem natural and anthropogenic aerosol emission datasets compared to biogenic emission data set. The biogenic emissions source data had a finer spatial resolution (1 km) than the background (1°) and anthropogenic (0.1°) emission source data. The 200 × 200 km size of the inner model domain means that the background emissions in particular, may not be well represented. Accordingly, anthropogenic gas phase sulphur-dioxide (SO_2) plume concentrations in ppmV were also used in this present study to represent anthropogenic aerosol. Anthropogenic SO_2 is a gaseous precursor to sulphate particles, one of the major anthropogenic aerosol constituents [4].

2.6. Data—Atmospheric Parameters

The spatial correlation of aerosol parameters and rain rate was also calculated in the context of atmospheric parameters known to influence the rain rate; cloud water content and vertical air motion. Cloud water content was represented by MODIS cloud integrated water path (CWP) in gm^{-2} at 1 km spatial resolution. CWP from the MODIS cloud product was derived from cloud optical thickness and cloud effective radius [57]. WRF-Chem provided the vertical wind (W) velocity parameter. The average vertical wind velocity (avW) was calculated from W values at each model level below the tropopause. Positive avW indicated ascending air and negative avW indicated descending air.

To evaluate the extent of orographic effects on precipitation in the study area, terrain height was compared with rain rate. Terrain elevation in meters above mean sea level was provided by Geosciences Australia 2001 maps with sub-kilometer horizontal spatial resolution and elevation vertical accuracy of ±150 m for 90% of points [58].

To evaluate the extent of urban environment enhanced surface temperature on precipitation in the study area, skin temperature (Kelvin) was extracted from WRF-Chem at 1 km spatial resolution.

To evaluate the extent of low level wind convergence on precipitation in the study area, wind field maps were created from WRF-Chem 10 m above ground level wind vectors (U, V) for each rain event. The wind maps were validated with Brisbane airport aerological diagrams provided by the BoM.

2.7. Methods

In order to compare aerosol emissions source classes with rain rate, four WRF-Chem models were run per rain event, with different aerosol emission configurations:

- all aerosol sources (background, biogenic, anthropogenic emissions);
- anthropogenic emissions only;
- background and anthropogenic aerosol emissions; and
- background and biogenic aerosol emissions.

WRF-Chem parameters (α, SO_2, W, surface temperature, U, V); terrain height; Doppler radar rain rate image files and MODIS CWP images were acquired, pre-processed and deposited into a geographic information system (GIS) known as ArcGIS; a software package manufactured by ESRI. ArcGIS routines were developed to extract the image and modeled variables to geo-referenced sample points at 1 km spatial resolution from model vertical levels below the tropopause, the location of which was determined from aerological diagrams. The Angstrom exponent (α) was calculated from the WRF-Chem AOD [59] at two wavelengths; 300 and 1000 nm, where λ is wave length:

$$\alpha_{\lambda 1/\lambda 2} = -\mathrm{Ln}(\mathrm{AOD}_{\lambda 1}/\mathrm{AOD}_{\lambda 2})/\mathrm{Ln}(\lambda 1/\lambda 2) \quad (1)$$

For each rain event a statistical sampling grid of 50 × 50 km at 1 km resolution was created in ArcGIS. The precise placement of the data grid depended on the location of modeled aerosol emissions with respect to a downwind rain band at MODIS overpass time. Each of the variables were extracted to the grid points and saved in geo-referenced text files suitable for spatial statistics processing in the "R", "Gstat" package.

We conducted two preliminary explorations of each data element to ensure they were suitable for spatial analysis using geostatistics. Each individual variable was tested for spatial autocorrelation within the sample grid by calculating Moran's I index using the "R" spatial statistics function library "ape". The tests established that similar values of each variable cluster together and at 99% certainly, the clustering is not by chance and spatial autocorrelation exists. Further, the type of statistical distribution of each variable was further assessed using "R" standard statistics libraries. Any skew from a Gaussian distribution was adjusted by logarithmic transformation as well as selecting an appropriate anisotropic cross-variogram calculation direction. Terrain elevation and surface temperature skew correction was also assisted by removing sample points over sea.

"Gstat" cross-variograms were calculated for each of the four model aerosol configurations comparing both α and SO_2 concentration with rain rate. These cross-variograms were then recalculated for the aerosol/rain data stratified for CWP above and below average CWP and avW representing descending and ascending air movement. Further cross-variograms were calculated comparing the spatial correlation of both terrain elevation and surface temperature and rain rate.

3. Results

3.1. Spatial Analysis—Correlation of Aerosol and Rain Rate

The following figures are maps of the variables used in the geostatistics for the extent of the sample grids and three rain events; rain rate (Figure 5) and four model configuration of α (Figure 6) and SO_2 (Figure 7). Experimental cross-variograms are presented (Figure 8) representing the joint spatial variability of both α and SO_2 with rain rate for three rain events and four model configurations.

Figure 5. BoM Mt Staplyton Doppler rain radar dimensionless rain intensity: (**a**) Sc2009, 2Dec09 03:48 UTC; (**b**) Cu/Sc2010, 25Sep10 03:40 UTC; and (**c**) St2011, 23Nov11 23:00 UTC showing the geostatistics sample grid extent for each.

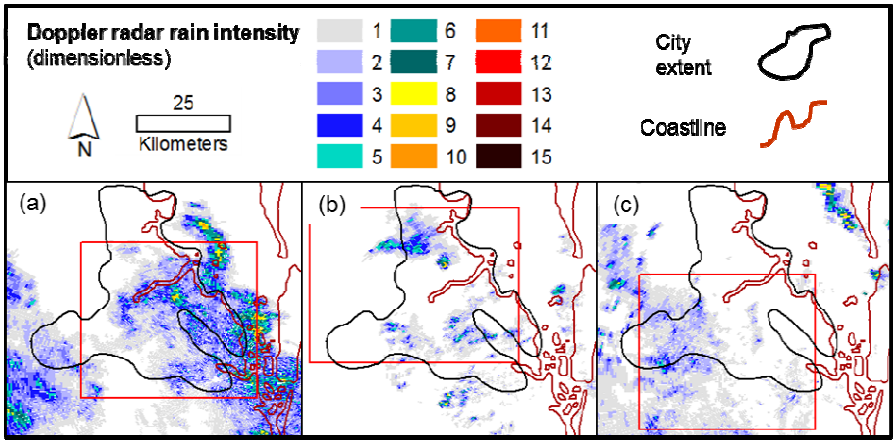

The cross-variograms for the Sc2009 event indicated that fine mode aerosol, represented by increasing α, was associated with decreasing rain intensity for the all-aerosol emissions model configuration. For the other three model configurations, decreasing aerosol size was associated with increasing rain intensity. The cross-variograms reached a sill at ranges of 10–18 km with an average range of 13.8 km. Similarly for the Cu/Sc2010 event, increasing α was associated with decreasing rain intensity for the all-aerosol emissions model configuration, and fine mode aerosol was associated with increasing rain intensity for the other three model configurations. All four Cu/Sc2010 cross-variograms reached a sill at a range of 21 km. For the St2011 rain event, all four cross-variograms indicated that fine mode aerosol was associated with decreasing rain intensity out to ranges of 21–25 km ranges with an average range of 23 km.

The inconsistent cross-correlation results for the two cumuliform rain events was reviewed by examining the spatial correlation of anthropogenic SO_2 and rain rate noting the earlier observation that WRF-Chem biogenic emissions may have skewed the model α output to fine model aerosol for the domains chosen such that background coarse mode aerosol may not be well represented. Firstly, maps of α and SO_2 were compared with each other before examining the cross-variograms with SO_2.

A visual comparison of α (Figure 6) and SO_2 emission concentration (Figure 7) maps for the "all aerosol" and "anthropogenic aerosol only" WRF-Chem aerosol transport scheme configurations indicated that the two proxies for aerosol size distribution used in this study are not well correlated. While not shown here, a cross-correlogram analysis indicated that at lag distances less than 10 km: (1) Sc2009 SO_2 was not correlated with α for either model configuration; (2) Cu/Sc2010 SO_2 was strongly negatively correlated with α for the "all aerosol" configuration (−0.58), and not correlated for the anthropogenic aerosol configuration; and (3) a moderate correlation existed for the two parameters (0.4) and both model configurations for the St2011 rain event. We noted that the underlying WRF-Chem urban land cover was not as extensive for Brisbane when compared with current maps of the city, which would also contribute to a model aerosol size distribution bias to biogenic emissions. An outcome for the geostatistics is that α and SO_2 were considered independent representations of aerosol size distribution and for the purposes of further discussion we concentrated on the SO_2 and rain rate relationships.

Figure 6. WRF Angstrom exponent for four aerosol transport scheme configurations and three rain events: (**a**–**d**) Sc2009; (**e**–**h**) Cu/Sc2010; and (**i**–**l**) St2011.

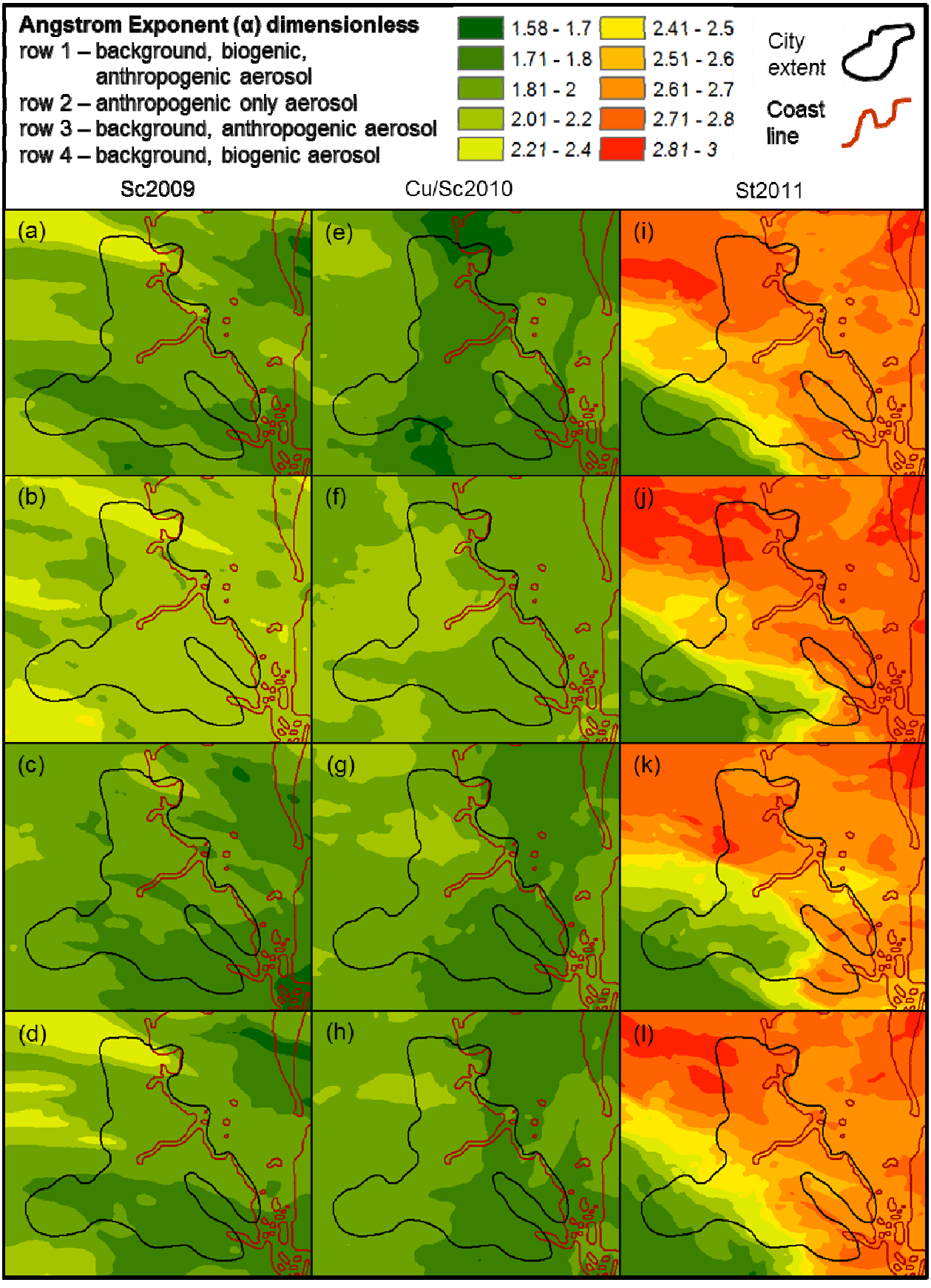

Figure 7. WRF sulphur dioxide (SO_2) emissions for four aerosol transport scheme configurations and three rain events: (**a**–**d**) Sc2009; (**e**–**h**) Cu/Sc2010 and (**i**–**l**) St2011.

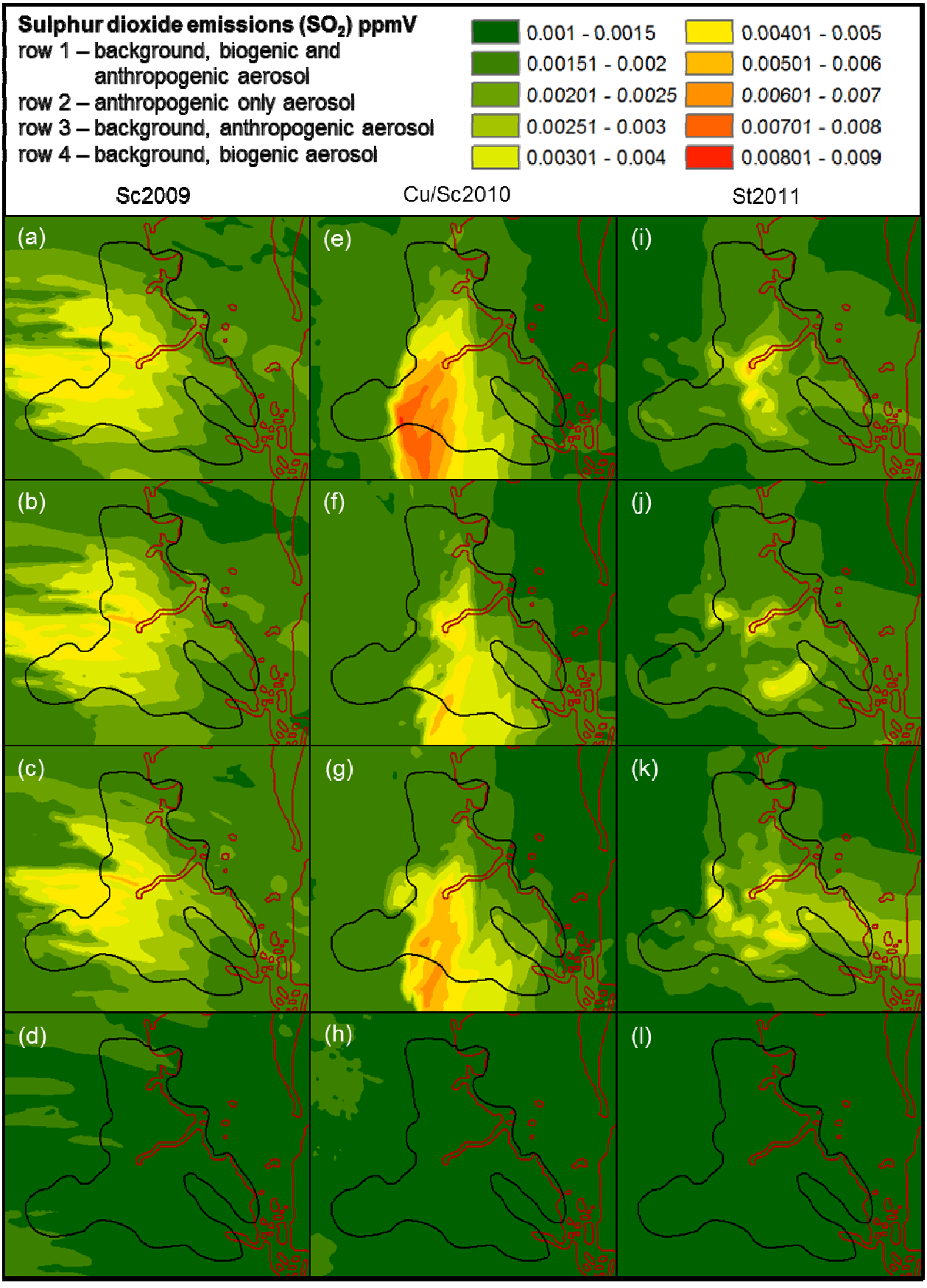

Figure 8. Cross-variograms for three rain events and four model configurations indicating the spatial correlation of logarithm transformed parameters—rain rate with both Angstrom exponent (α) and SO_2 emissions: Sc2009 (**a**,**g**,**m**,**s**) α and (**b**,**h**,**n**,**t**) SO_2; Cu/Sc2010 (**c**,**i**,**o**,**u**) α and (**d**,**j**,**p**,**v**) SO_2: St2011 (**e**,**k**,**q**,**w**) α and (**f**,**l**,**r**,**x**) SO_2.

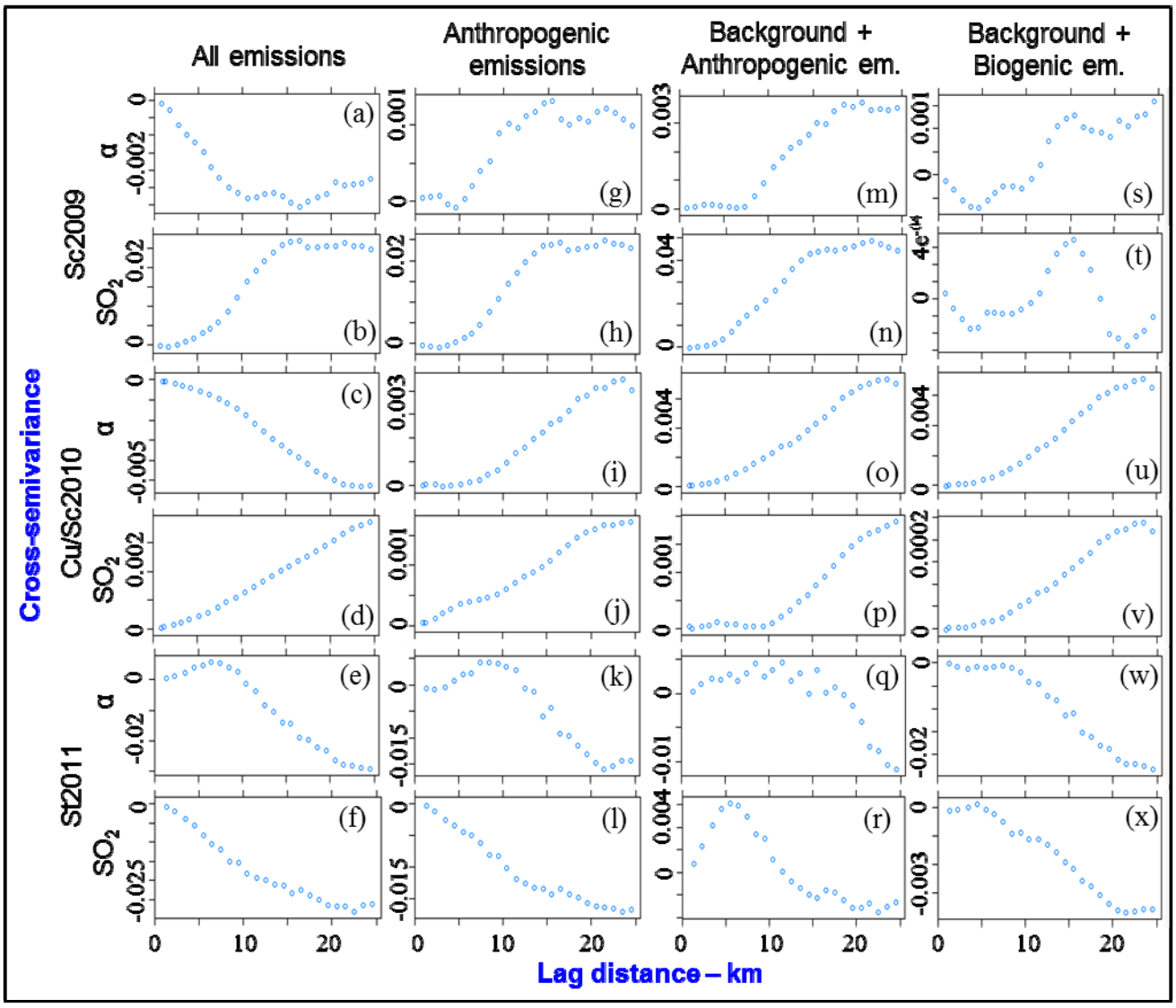

The cross-variograms for the Sc2009 event indicated for three model configurations: all emissions, anthropogenic only emissions, and background/anthropogenic emissions, that increasing anthropogenic SO_2 was associated with increasing rain intensity. The cross-variogram for background and biogenic SO_2 emissions (Figure 8t) showed an inconclusive spatial relationship with rain rate—the cross-variogram did not reach a definite sill denoting little or no spatial cross-correlation. This is due to SO_2 being primarily of anthropogenic origin and, therefore, largely absent from this model configuration. This is a more consistent result than the Sc2009 cross-variograms for α and rain rate. The three cross-variograms for the Sc2009 SO_2/rain rate association indicated their spatial relationship reached a sill from ranges of 15–17 km with an average range of 15.3 km.

All four cross-variograms for the Cu/Sc2010 event showed that increasing SO_2 was associated with increasing rain intensity. For the background and biogenic emissions model configuration, the semi-variance sill value was an order of magnitude less than for the other three cross-variograms

indicating the relationship has less strength due to the absence of anthropogenic SO_2. The three cross-variograms for the Cu/Sc2010 SO_2/rain rate association indicated their spatial relationship reached a sill from ranges of 22–25 km with an average range of 24 km. While not readily apparent, Figure 8d,p do sill at 25 km verified from graphs with 40 km of lag distance not shown here to maintain figure clarity.

For the St2011 rain event, three cross-variograms—all-aerosol emissions, anthropogenic only emissions and background/biogenic emissions—showed that SO_2 was negatively correlated with rain intensity. These three cross-variograms reached a sill at ranges from 21–25 km, an average range of 23 km. Different to these three cross-variograms, the background/anthropogenic emissions model cross-variogram had a semivariance that spiked to a short range positive semi-variance at 5 km, indicating the importance of biogenic emissions to the fine mode aerosol fraction in the WRF-Chem configuration to the structure of the other three cross-variograms.

3.2. Spatial Analysis—Stratified for Cloud Water Content and Vertical Air Movement

Putting aside the cross-variograms of α and rain-rate, we compared the cross-variograms of unconstrained SO_2/rain rate with those constructed from the sample grid data stratified for: (1) above and (2) below average MODIS CWP (Figure 9); and (3) ascending and (4) descending vertical air movement (Figure 10). The intention of this analysis was to see if cloud water content or vertical air movement could counter explain the SO_2 and rain rate relationships described earlier. The cross-variograms shown here are for the "all aerosol" WRF-Chem configuration (Figure 11). A visual comparison of cross-variograms for stratified data sets with the non-stratified data set indicates the extent to which grid point location clustering dictates the spatial relationships of aerosol size and rain intensity. The non-stratified data set was collected from regular 1 km sample grid, whereas the stratified data sets are irregular, sometimes with distances of 5 km between clusters. The significant "hole effects" in the cross-variograms are a result of the non-grid nature of the stratified data sets.

Figure 9. MODIS Cloud Water Path (CWP) for three rain events: (**a**) Sc2009, (**b**) Cu/Sc2010 and (**c**) St2011.

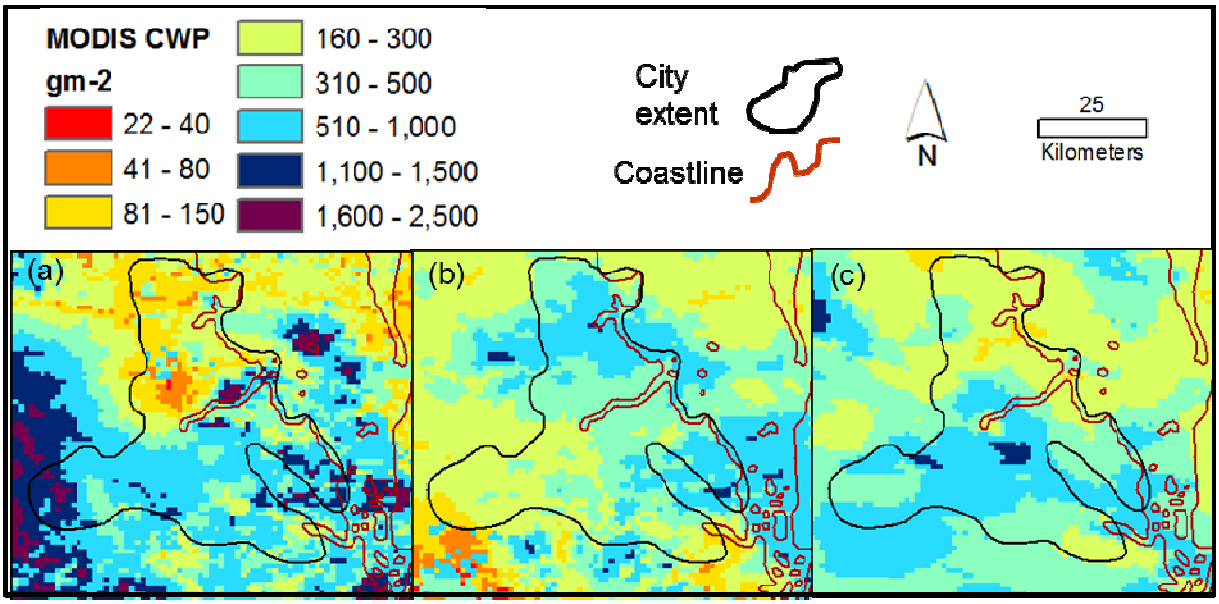

Figure 10. WRF mean below tropopause vertical wind speed for three rain events: (**a**) Sc2009, (**b**) Cu/Sc2010 and (**c**) St2011.

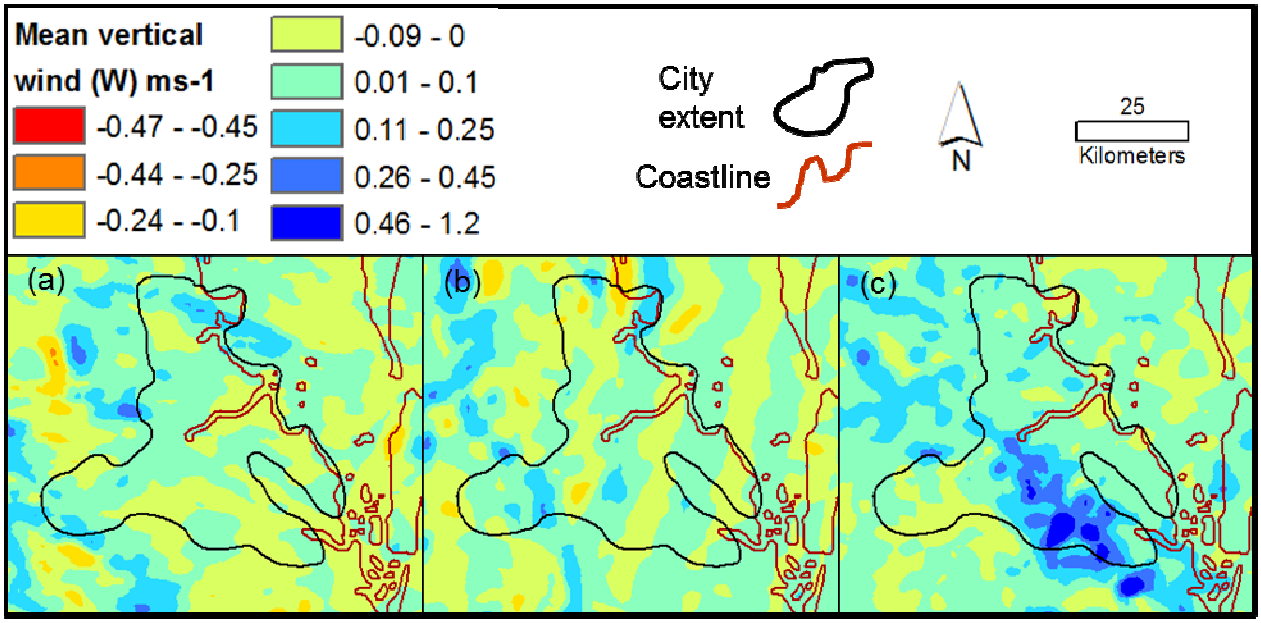

Figure 11. All aerosol model cross-variograms for three rain events indicating the spatial correlation of logarithm transformed rain rate with SO_2 emissions for: (**a**,**f**,**k**) all grid points; and grid data points stratified for: (**b**,**g**,**l**) column average vertical wind movement (avW) less than or equal to 0 ms-1; (**c**,**h**,**m**) avW >0 ms-1; (**d**,**i**,**n**) cloud water path (CWP) ≤average CWP; and (**e**,**j**,**o**) CWP >average CWP.

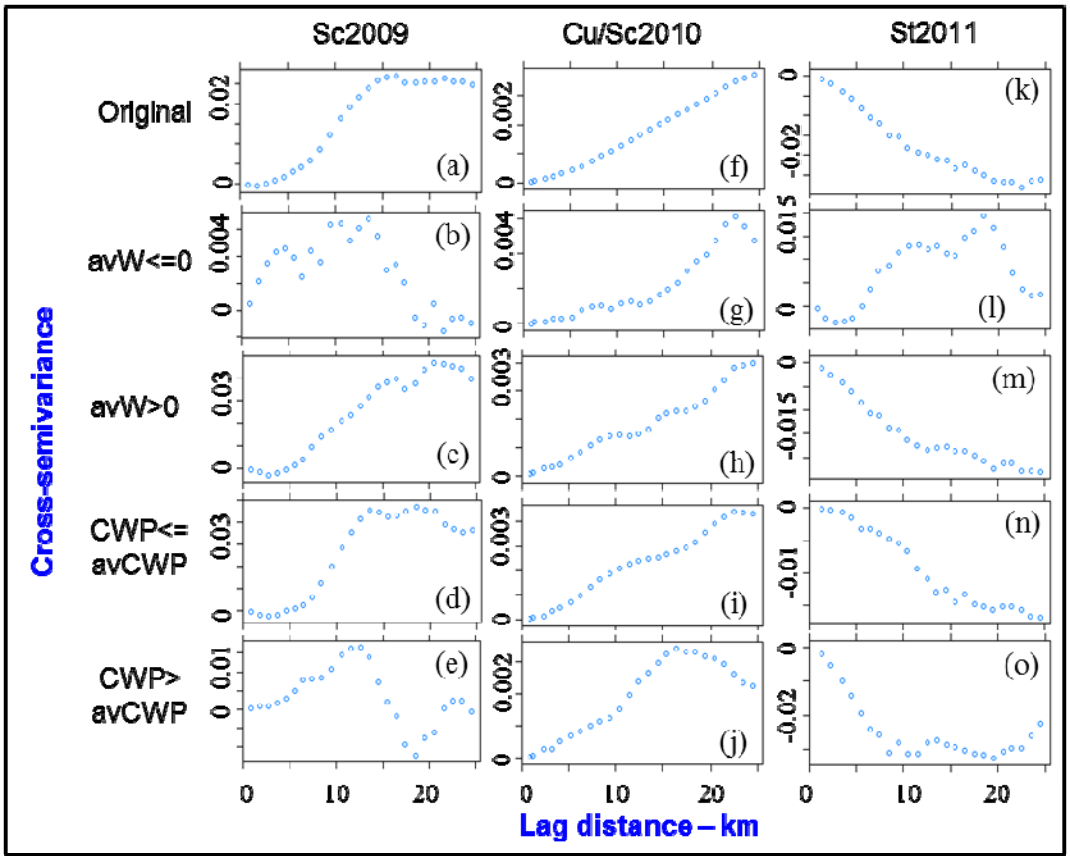

Sorooshian *et al*. [60] found for shallow cumulus clouds that the CWP threshold at which there is sufficient cloud water to sustain precipitation regardless of aerosol size distribution is 1000 gm^{-2}. Since the MODIS CWP images indicates only comparatively small areas where CWP is greater than 1000 gm^{-2} inside the extent of the sample grids (Figure 5), the amount of cloud water of each rain event was probably not sufficient to rule out aerosol indirect effects on rainfall.

For the Sc2009 rain event, all five SO_2/rain-rate cross-variograms (Figure 11), from the original un-stratified and the four stratified data sets, indicate that increasing concentration of SO_2 is associated with increasing rain-rate. The cross-variograms with CWP, periodicity aside, have a similar structure and semi-variance sill values which suggests that the association between rain-rate and SO_2 emissions are, for the most part, not sensitive to CWP. The less than average CWP has a cross-variogram structure similar to the unconstrained data cross-variogram indicating that the SO_2 and rain rate may have a primary association when there is less cloud water available. This subtlety of the geostatistics suggests that increasing SO_2 emissions, via smaller secondary particle creation, may be associated with increasing rain rate when there is less competition for precipitation processes or delaying the growth of cloud droplets in the warm phase and providing more droplets for the ice phase process. The Sc2009 avW rising air stratified cross-variogram structure and semi-variance sill value is most similar to the non-stratified data cross-variogram. This indicates that the SO_2/rain rate association is primarily in rising air as expected.

For the Cu/Sc2010 rain event, the SO_2/rain-rate cross-variograms stratified with CWP greater than average CWP values reached a sill at 16 km rather than 22 km for the cross-variogram stratified with CWP less than average CWP. The less than average CWP stratified cross-variogram is similar in structure to the non-stratified cross-variogram indicating that this stratification is the dominant data set—similar to the SC2009 event. Since both CWP stratified and original SO_2/rain rate cross-variograms have a similar structure, and periodicity aside, the association between these variables is not particularly sensitive to CWP. This observation holds for both "all aerosol" and "anthropogenic aerosol only" model aerosol transport configurations. The Cu/Sc2010 avW cross-variograms have a similar structure and sill value to the non-stratified cross-variogram indicating for this event, that the SO_2/rain rate association is not particularly sensitive to vertical air movement.

Comparing the non-stratified and stratified SO_2/rain rate cross-variograms for the St2011 rain event indicates that there is little sensitivity to CWP—but a primary relationship in ascending air. The association of fine mode aerosol with decreasing rain rate has a 10–15 km longer range when CWP is greater than average CWP in the sampling grid. This suggests that anthropogenic emissions influence the particle uptake of water in warm phase clouds by 10–15 km.

3.3. Spatial Analysis—Potential Alternative Correlations

The following ArcGIS maps show Earth surface temperature (Figure 12) and terrain elevation (Figure 13) for the three rain event sampling grid extents. The related cross-variograms (Figure 14) illustrate the spatial correlation of those two variables with rain rate.

Figure 12. Earth Surface (skin) Temperature at the time of rain rate observation for three rain events (**a**) Sc2009, (**b**) Cu/Sc2010, and (**c**) St2011.

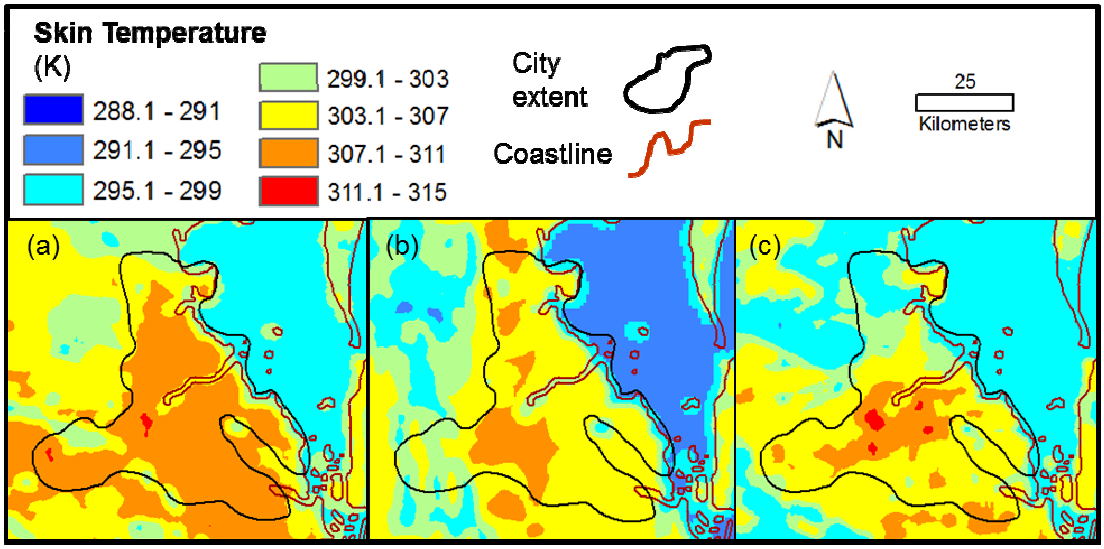

Figure 13. Terrain elevation for the extent of the study area.

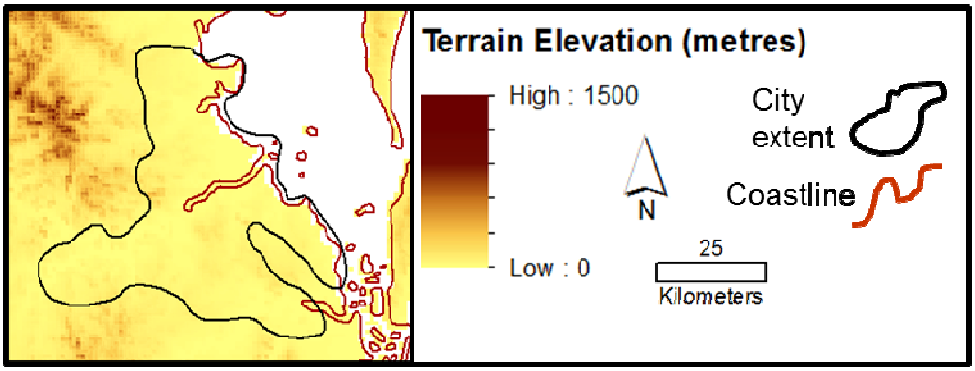

Figure 14. Cross-variograms indicating the spatial correlation for skin temperature and rain rate (**a**–**c**) and terrain elevation and rain rate (**d**–**f**) for three rain events.

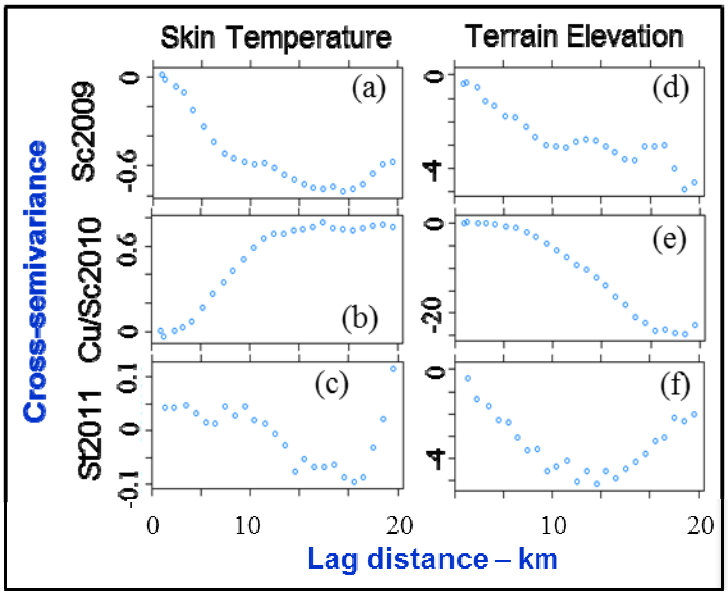

The terrain elevation/rain rate cross-variograms indicated consistent negative correlations for each rain event: to a range of 24 km for the Sc2009 event, 20 km for the Cu/Sc2010 event and 12 km for the St2011 event. Accordingly, increasing terrain height was associated with decreasing rain intensity.

The surface temperature/rain intensity cross-variograms indicated a negative correlation for the Sc2009 event to a range of 18 km; a positive correlation to 12 km for the Cu/Sc2010 system and an indeterminate relationship for the St2011 rain event.

While not shown here, the WRF-Chem winds at 7 km above ground level for all three rain events showed that the winds aloft were driving the cloud bearing rain in westerly or north-westerly air flow, consistent with the movement of rainfall in the time series of Doppler rain radar images as well as Brisbane airport aerological diagrams. The low level wind maps (Figure 15) for the Sc2009 and Cu/Sc2010 rain events did not indicate any low level wind convergence within the statistics grids or in the vicinity of Brisbane city generally. For the St2011 event a low level wind convergence was noted as wind from the north-east met a southerly wind change coincident with the position of a surface trough separating two high pressure systems.

Figure 15. WRF wind speed and direction at 10 m above ground level for three rain events: (**a**) Sc2009, (**b**) Cu/Sc2010, and (**c**) St2011.

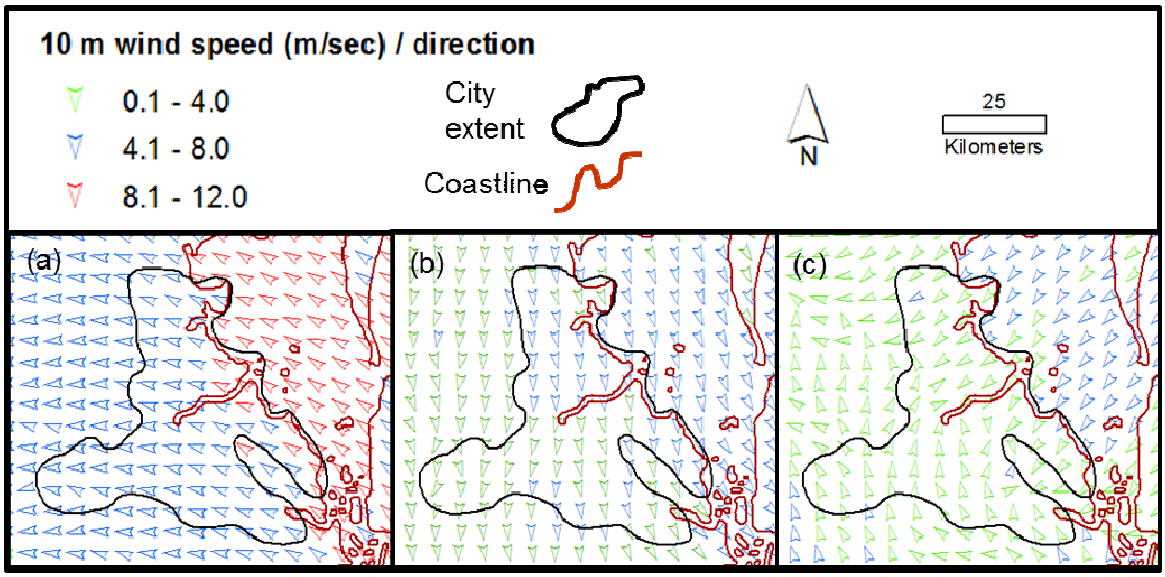

4. Discussion

4.1. Spatial Analysis—Correlation of Aerosol and Rain Rate

Geostatistics applied to the St2011 rain event point to both fine mode aerosol fraction and increasing anthropogenic SO_2 emissions having a spatial and temporal association with areas of decreasing rain intensity downwind of anthropogenic aerosol emissions. For the two cumuliform rain systems studied, the geostatistics consistently indicated that increasing anthropogenic SO_2 concentration was related to increasing rain intensity, with limited spatial co-variation beyond 15 km. The cumuliform geostatistics comparing α and rain intensity was less clear. For both cumuliform events the geostatistics indicated that areas of decreased aerosol size in the "all emissions" configuration were related to areas of decreasing rain intensity. However, the other three model

configurations indicated that decreasing aerosol size was related to areas with increasing rain intensity. The SO_2/rain rate cross-variograms reached higher cross-semivariance sill values than those for α/rain rate indicating that WRF-Chem SO_2 emission data has a more normal distribution function than the α data across the sampling grid. Accordingly, we place more interpretative weight on the SO_2 cross-variograms. While the time duration for gas phase SO_2 molecule reactions to create hygroscopic aqueous sulfuric acid particles is variable and although part of the process occurs rapidly in the presence of water vapour [19], SO_2 residence times in the atmosphere is around four days [61]. This means the use of SO_2 as a proxy for anthropogenic aerosol is not ideal. However, the source location of anthropogenic aerosol is made explicit for the spatial analysis using SO_2 emissions whereas the source location of WRF-Chem-generated secondary anthropogenic aerosol species would be unclear.

The geostatistics for both cumuliform events indicates that increasing anthropogenic SO_2 concentration is related to increasing rain intensity. The Sc2009 event SO_2 and rain intensity spatial correlation has an order of magnitude higher sill than that for the Cu/Sc2010 event indicative of the greater range in the rain-rate values for the first rain event. The stronger SO_2/rain rate association for the Sc2009 system might be explained by the larger divergence in the rain rate assisting clearer cross-variogram structure. The SO_2/rain rate relationship for the Cu/Sc2010 system exists for a longer range, exhausting joint variance at around 22 or 25 km rather than the Sc2009 system at 10 km. MODIS cloud top pressure images showed that the Sc2009 Sc layer had deeper convective cells embedded within it. At around 620 hPa, these cells were some 3 km thick signifying turbulent mixing aided collision and coalescence processes. The Cu/Sc2010 observations indicated comparatively more isolated Cu cells with less chance of ice phase invigoration by delayed processing of water droplets from the warm phase.

Considering all aerosol emissions, the lag distances between sample points for which aerosol and rain intensity retain a correlation are: St2011—23 km; Cu/Sc2010—21 km; and Sc2009—10 km. The average distance for the aerosol effect on rain intensity is 18 km from aerosol ingestion. Similarly for anthropogenic only aerosol emissions: St2011—21 km; Cu/Sc2010—21 km; and Sc2009—12 km, an average 18 km. For both model configurations, the distances over which SO_2 emissions and rain intensity retain a correlation are: St2011—20 km; Cu/Sc2010—25 km; and Sc2009—15 km with an average 20 km. The relationship between anthropogenic aerosol and rain intensity for the rain events studied exists between 12 and 25 km depending on cloud type and structure. These geostatistical correlation distances are consistent with Han *et al*. [14] who determined, using the two dimensional non-hydrostatic Hebrew University Cloud Model, that anthropogenic aerosol enhanced cumuliform rainfall was evident 20 km downwind of pollution emission sources.

4.2. Spatial Analysis—Potential Alternative Correlations

The negative correlation of terrain elevation and rain intensity indicated by the cross-variogram analysis for all three rain events (Figure 14) is possibly consistent with descending and warming air movement enhancing evaporation and rain dispersal. However, the precipitation within the extent of the sample grids was on the downwind side of the higher terrain for all three rain events since the rain bearing clouds are being steered by north-westerly winds aloft. This geostatistical indication that

aerosol and rain rate associations are not counter explained by orographic effects is further discussed for each rain event studied.

For Sc2009 the 10 m wind direction was from the south-east (Figure 15a) toward the area of higher terrain west of Brisbane—a possible orographic enhancement. The WRF-Chem modeled vertical wind velocities (W) at 1.5 km above ground level, close to the Sc cloud base of the rain event in the area of the statistics sampling grid, indicated disparate gentle vertical air motion between −0.01–0.03 ms^{-1}, which indicated an orographic wind enhancement was unlikely. Further, wind measurements from an automatic weather station situated within the extent of the sampling grid indicated light and variable winds from 03:00–04:00 UTC. The images of WRF-Chem avW (Figure 10a) and the location of rain intensity (Figure 5a) with respect to cumulous cloud tops embedded in the strato-cumulus cloud layer (Figure 2), indicated that the vertical air movement regime in, and around the statistical sampling grid, was associated with cumuliform cloud rather than orographic lifting.

For Cu/Sc2010 the 10 m winds from the north (Figure 15b) did not provide any evidence of orographic lifting. The modeled vertical wind velocities (W) at 1.5 km above ground level, close to the cloud base of the rain event in the area of the statistics sampling grid, indicated gentle vertical air motion between −0.06 to 0.14 ms^{-1} with a spatial distribution (Figure 10b) suggesting the vertical air movement is associated with cumuliform cloud processes.

The 10 m wind direction within the area of the statistics grid for the St2011 system (Figure 15c) indicated some low level convergence of air flow. Such atmospheric dynamics works to enhance stratiform rain and is consistent with the location of the radar observed rainfall. The WRF-Chem vertical wind velocities image (Figure 15c) showed weakly rising air of 0.03 ms^{-1} at 240 m above ground level in and around the sampling grid, typical of a stratiform system for the extent of the sampling grid ruling out terrain lee side downward air movement. As a result we conclude that for the three rain events studied, it is unlikely that orographic lifting processes counter explain the geostatistical associations of aerosol and rain intensity found in the study.

For the Sc2009 system, an increasing surface temperature is related to decreasing rain intensity (Figure 14a). An aerological diagram for Brisbane airport shows an unstable atmosphere below 900 hPa; a capping inversion at 800 hPa; a lifted index value of 1.73 °C; and a convective available potential energy value of 5.62 jKg^{-1}, all indicating a low chance of storm development. However, cumuliform rain was widespread and just as intense west as it was east of the city (Figure 2) suggesting rain-fall would be self-sustaining regardless of the urban environment enhanced surface temperatures in accordance with findings from Dixon and Mote [62]. Taken together, the urban environment enhanced surface temperature does not counter explain the Sc2009 rain event anthropogenic aerosol association with increased rainfall.

For the Cu/Sc2010 system, and different to the Sc2009 system, the geostatistics (Figure 14b) indicates that urban surface temperature were associated with areas of increased rain intensity. A Brisbane airport aerological diagram indicated generally unstable atmosphere conditions below 1,000 m with a lifted index value of 1.64 °C and a convective available potential energy value of 3.21 jKg^{-1} indicative of low probabilities for convective storm development. The relative humidity for the afternoon of September 25, 2010 ranged from 64%–68%. These conditions are suitable for an urban environment effect on rainfall as defined by Dixon and Mote [62]. Since the isolated rainfall of the Cu/Sc2010 event is generally located slightly east of the city of Brisbane only (Figure 3), the

enhanced urban environment surface temperature influence on decreasing rain rate cannot be ruled out for the Cu/Sc2010 rain event.

The spatial analysis suggests that enhanced surface temperature of the built environment is probably not associated with drying the atmosphere and thus counter explaining the St2011 rain event anthropogenic aerosol association with decreasing rainfall. The inconclusive cross-variogram structure (Figure 14c) indicates little correlation at any distance between land surface temperature and rain intensity.

The modeled 10 m above ground level wind maps for the two cumuliform rain systems (Figure 15a,b) do not indicate any wind convergence lifting mechanism in the vicinity of the Brisbane city. In addition, the modeled vertical wind velocities at 10/240 m and a central point of the statistics grid was low: (1) Sc2009—0.01/0.04 ms^{-1}; and (2) Cu/Sc2010—0/0 ms^{-1} respectively. Further, modeled vertical wind velocities areal images showed generally homogenous values of vertical air motion at these heights. Since the low level vertical motion of the atmosphere for these rain events is negligible, wind convergence is unlikely to counter explain the aerosol size distribution and rainfall relationships found for the cumuliform rain systems.

The model 10 m above ground level for the St2011 system shows a low level wind convergence zone, possibly marking a weak pressure trough. However, the model indicates weak vertical wind velocities at low levels: 0 ms^{-1} at 10 m and 0.03 ms^{-1} at 240 m above ground level. Since low level wind convergence would enhance stratiform rainfall it is unlikely wind convergence counter explains the geostatistics result that anthropogenic aerosol is associated with decreasing rainfall intensity for this stratiform rain event.

4.3. Spatial Analysis—General Comments

While it is clear that the WRF-Chem setup for the Brisbane study area has a bias in the fine mode aerosol output due to the varying spatial resolutions of the global aerosol emission data sets, the geostatistics from different model configurations suggests that the fine mode aerosol effects on rainfall are similar whether they are from anthropogenic or biogenic sources—particle size rather than aerosol species appears to be the determining factor. The cross-variograms, for which the fine mode is predominately of either anthropogenic or biogenic origin, are generally similar. The caveat is that the database of natural background aerosol used in WRF-Chem had a coarse spatial resolution. In addition, the age of the anthropogenic aerosol databases represents a limitation to the spatial analysis.

A natural question that arises from this research is: does the pollution effect on rain intensity mean that Brisbane water supply receives less rainfall than it would if the pollution emanating from urbanized activity did not exist? Our conjecture is probably not. Stratiform rain systems form some 45% of all rain events for Brisbane either from summer monsoon egress from the north-west of Brisbane or from winter moist westerly geostrophic winds. Since Brisbane's water catchments are located west of both the city and nearby higher terrain, and given that pollution inhibiting rainfall would take place east of the city in such regimes, the impact on Brisbane's water storage is unlikely. South-easterly trade wind stratocumulus systems may be impacted by the aerosol effect on rainfall; however, most rainfall from these regimes occurs on the eastern side of higher terrain and generally do not impact Brisbane's water catchments.

For larger cities around the globe or for areas where industrial activity is concentrated and where stratiform rain bearing systems predominate, the question of whether anthropogenic aerosol has an impact on water supply may well be significant.

5. Conclusions and Further Work

Using remote sensing observations, weather modelling and geostatistics, this study investigated the spatial relationship between aerosol species and rain intensity around Brisbane, a sub-tropical Australian city.

Universal co-kriging cross-variograms characterised the spatial relationships between aerosol size distribution represented by two modelled proxies—Angstrom exponent and sulphur dioxide concentration—with individual rain event Doppler radar reflectivity derived rain intensity for 2,500 km^2 grids at 1 km spatial resolution. The cross-variograms of the three case study events suggest that smaller pollution particles are associated with decreasing rain intensity for the single stratiform system studied. For cumuliform systems, cross-variograms with SO_2 concentrations indicate anthropogenic emissions may enhance rain intensity. The distance to which anthropogenic aerosol affects rain rate varies from 12–25 km, depending on cloud type. For three rain events studied, results confirm an emerging consensus that anthropogenic aerosol affects rainfall in different ways depending on cloud structure.

Recalculated cross-variograms of SO_2 emissions and rain rate stratified by proxies for cloud water content and vertical wind velocities indicated that these atmospheric parameters are unlikely to counter explain the fine mode aerosol effects on rain intensity for the particular rain events studied.

Within the same statistics sample grid used for exploring aerosol size distribution and rain rate associations, three thermal and dynamical processes that influence rainfall were further investigated: orographic lifting, convection influenced by the built environment as a result of enhanced (higher) surface temperatures and low level wind convergence. The geostatistics, as well as the rain location, indicate orographic effects do not counter explain the relationship of aerosol size distribution and rain intensity. The geostatistics also suggest that enhanced urban surface temperatures do not influence the stratiform and one cumuliform rain rate, but an influence cannot be ruled out for the other cumuliform rain rate. It is also unlikely that wind convergence counter explains the relationship of anthropogenic aerosol and rain intensity for these three rain events.

Our study shows that the application of geostatistics complements existing research into aerosol effects on rainfall. Clearly geostatistics should be applied to many more rain events at the city extent—1 km spatial resolution per rain event temporal scale—to confirm aerosol effects on rainfall. Although this research found single cloud layers co-located with Brisbane aerosol emissions areas at satellite overpass difficult to find for the period 2009–2011, comparing 1 km spatial resolution satellite observed cloud effective radius with aerosol emissions using geostatistics is a worthwhile goal. Research should also include a measurement campaign that separates anthropogenic and biogenic fine mode fractions to confirm that small sized aerosol from either source affects precipitation in a similar way. A limitation of the study was the inability of the "R" Gstat package to produce cross-variogram "hulls of perfect correlation" [27]. This capability would have been useful to determine the strength of the spatial correlation of study variables. In Australia research on the effects of aerosols on

precipitation would greatly benefit from an inventory of anthropogenic aerosol emissions at 1 km spatial resolution which would separate transport corridors and individual hubs of industry. Equally important would be the creation of an updated land-use scheme and erodibility index specific to Australia at a finer spatial resolution than those available for WRF-Chem aerosol emissions databases. We suggest that research is directed into these two areas as matter of urgency to advance understanding of the aerosol effect on precipitation processes. The new datasets to emerge would enable improved accuracy of future predictions of rainfall in the most water scare inhabited continent.

Acknowledgments

The authors thank: The Queensland Government Smart Futures fund; The University of Queensland Graduate School travel award; NCAR/NOAA scientists for WRF/WRF-Chem and NASA mission scientists and personnel for MODIS data.

Conflicts of Interest

The authors declare no conflict of interest.

References

1. Ahrens, C.D. *Essentials of Meteorology: An Invitation to the Atmosphere*, 6th ed.; Brooks/Cole Cengage Learning: Belmont, CA., USA, 2012.
2. Forster, P.; Ramaswamy, V.; Artaxo, P.; Berntsen, T.; Betts, R.; Fahey, D.W.; Haywood, J.; Lean, J.; Lowe, D.C.; Myhre, G.; *et al*. *Changes in Atmospheric Constituents and in Radiative Forcing*; Intergovernmental Panel on Climate Change: Cambridge, UK, New York, NY, USA, 2007.
3. Levin, Z.; Cotton, W.R. *Aerosol Pollution Impact on Precipitation, A Scientific Review*; Springer, 2009.
4. Andreae, M.O.; Rosenfeld, D. Aerosol-cloud-precipitation interactions. Part 1, The nature and sources of cloud-active aerosols. *Earth Sci. Rev.* **2008**, *89*, 13–41.
5. Warner, J. A reduction in rainfall associated with smoke from suger-cane fires—An inadvertent weather modification? *J. Appl. Meteorol.* **1968**, *7*, 247–251.
6. Rosenfeld, D. Suppression of rain and snow by urban and industrial air pollution. *Science* **2000**, *287*, 1793–1796.
7. Bigg, E.K. Trends in rainfall associated with sources of air pollution. *Environ. Chem.* **2008**, *5*, 184–193.
8. Jin, M.; Shepherd, J.M.; King, M.D. Urban aerosols and their variations with clouds and rainfall: A case study for New York and Houston. *J. Geophys. Res.* **2005**, *110*, 1–12.
9. Lacke, M.C.; Mote, T.L.; Shepherd, J.M. Aerosols and associated precipitation patterns in Atlanta. *Atmos. Environ.* **2009**, *43*, 4359–4373.
10. Koren, I.; Altaratz, O.; Remer, L.A.; Feingold, G.; Martins, J.V.; Heiblum, R.H. Aerosol-induced intensification of rain from the tropics to the mid-latitudes. *Nat. Geosci.* **2012**, *5*, 118–122.
11. Van den Heever, S.C.; Cotton, W.R. Urban aerosol impacts on downwind convective storms. *J. Appl. Meteorol. Climatol.* **2007**, *46*, 828–850.

12. Yang, Q.; Gustafson, W.I., Jr.; Fast, J.D.; Wang, H.; Easter, R.C.; Wang, M.; Ghan, S.J.; Berg, L.K.; Leung, L.R.; Morrison, H. Impact of natural and anthropogenic aerosols on stratocumulus and precipitation in the Southeast Pacific: A regional modelling study using WRF-Chem. *Atmos. Chem. Phys. Discuss.* **2012**, *12*, 14623–14667.
13. Lohmann, U. Global anthropogenic aerosol effects on convective clouds in ECHAM5-HAM. *Atmos. Chem. Phys.* **2008**, *8*, 2115–2131.
14. Han, J.-Y.; Baik, J.-J.; Khain, A.P. A numerical study of urban aerosol impacts on clouds and precipitation. *J. Atmos. Sci.* **2012**, *69*, 504–520.
15. Lin, Y.; Min, Q.; Zhuang, G.; Wang, Z.; Gong, W.; Li, R. Spatial features of rain frequency change and pollution and associated aerosols. *Atmos. Chem. Phys. Discuss.* **2011**, *11*, 8747–8776.
16. Zhang, L.; Liao, H.; Li, J. Impacts of Asian summer monsoon on seasonal and interannual variations of aerosols over eastern China. *J. Geophys. Res.: Atmos.* **2010**, *115*, doi:10.1029/2009JD012299.
17. Khain, A.P.; BenMoshe, N.; Pokrovsky, A. Factors determining the impact of aerosols on surface precipitation from clouds: An attempt at classification. *J. Atmos. Sci.* **2008**, *65*, 1721–1748.
18. Lee, S.S.; Penner, J.E.; Saleeby, S.M. Aerosol effects on liquid-water path of thin stratocumulus clouds. *J. Geophys. Res.* **2009**, *114*, doi:10.1029/2008JD010513.
19. Seinfeld, J.H.; Pandis, S.N. *Atmospheric Chemistry and Physics From Air Pollution to Climate Change*, 2nd ed.; John Wiley and Sons: Hoboken, NJ., USA, 2006.
20. Lin, Y.; Min, Q.; Zhuang, G.; Zhuang, Z.; Gong, W.; Li, R. Spatial features of rain frequency change induced by pollution and aossociated aerosols. *Atmos. Chem. Phys. Discuss.* **2010**, *10*, 14495–14511.
21. Ayers, G. Air pollution and climate change: Has air pollution suppressed rainfall over Australia? *J. Clean Air Soc. Aust. N. Z.* **2005**, *39*, 51–57.
22. Ayers, G. Air pollution and precipitation suppression over SE Australia: Critical review of evidence presented by Rosenfeld (2000) and Rosenfeld (2006). *Tellus* **2009**, *61B*, 685–693.
23. Qin, Y.; Mitchell, R.M. Characterisation of episodic aerosol types over the Australian continent. *Atmos. Chem. Phys.* **2009**, *9*, 1943–1956.
24. Chan, Y. *Identification of Sources of $PM_{2.5}$ and PM_{10} Aerosols in Brisbane*; Griffith University: Brisbane, Australia, 1997.
25. Cheung, H.C.; Morawska, L.; Ristovski, Z.D. Observation of new particle formation in subtropical urban environment. *Atmos. Chem. Phys.* **2011**, *11*, 3823–3833.
26. Goovaerts, P. *Geostatistics for Natural Resources Evaluation*; Oxford University Press: New York, NY., USA,1997.
27. Webster, R.; Oliver, M.A. *Geostatistics for Environmental Scientists*, 2nd ed.; John Wiley and Sons: Chichester, West Sussex, England, 2007.
28. Grimes, D.I.F.; Pardo-Iguzquiza, E. Geostatistical analysis of rainfall. *Geogr. Anal.* **2010**, *42*, 136–160.
29. Chappell, A. An Introduction to Geostatistics. In *Key Methods in Geography*, 2nd ed.; Clifford, N., French, S., Valentine, G., Eds.; SAGE: London, Great Britain, 2010.
30. Pebesma, E.J. Multivariable geostatistics in S: The GSTAT package. *Comp. Geosci.* **2004**, *30*, 683–691.

31. Bostan, P.A.; Heuvelink, G.B.M.; Akyurek, S.Z. Comparison of regression and kriging techniques for mapping the average annual precipitation of Turkey. *Int. J. Appl. Earth Obs. Geoinf.* **2012**, *19*, 115–126.
32. McComiskey, A.; Feingold, G. The scale problem in quantifying aerosol indirect effects. *Atmos. Chem. Phys.* **2012**, *12*, 1031–1049.
33. Yu, X.; Zhu, B.; Zhang, M. Seasonal variability of aerosol optical properties over Beijing. *Atmos. Environ.* **2009**, *43*, 4095–4101.
34. Sheridan, P.J.; Andrews, E.; Ogren, J.A.; Tackett, J.L.; Winker, D.M. Vertical profiles of aerosol optical properties over Central Illinois and comparison with surface and satellite measurements. *Atmos. Chem. Phys. Discuss.* **2012**, *12*, 17187–17244.
35. Chin, M.; Ginoux, P.; Kinne, S.; Torres, O.; Holben, B.N.; Duncan, B.N.; Martin, R.V.; Logan, J.A.; Higurashi, A.; Nakajima, T. Tropospheric aerosol optical thickness from the GOCART model and comparisons with satellite and sun photometer measurements. *J. Atmos. Sci.* **2002**, *59*, 461–483.
36. Dusek, U.; Frank, G.P.; Hildebrandt, L.; Curtius, J.; Schneider, J.; Walter, S.; Chand, D.; Drewnick, F.; Hings, S.; Jung, D.; *et al*. Size matters more than chemistry for cloud-nucleating ability of aerosol particles. *Science* **2006**, *312*, 1375–1378.
37. Rosenfeld, D. Aerosols, clouds and climate. *Science* **2006**, *312*, 1323–1324.
38. Grell, G.A.; Peckham, S.E.; Schmitz, R.; McKeen, S.A.; Frost, G.; Skamarock, W.C.; Eder, B. Fully coupled "online" chemistry within the WRF model. *Atmos. Environ.* **2005**, *39*, 6957–6975.
39. Remer, L.A.; Kaufman, Y.J.; Tanre, D.; Mattoo, S.; Chu, D.A.; Martins, J.V.; Li, R.-R.; Ichoku, C.; Levy, R.C.; Kleidman, R.G.; *et al*. The MODIS aerosol algorithm, products, and validation. *J. Atmos. Sci.* **2005**, *62*, 947–973.
40. Drury, E.; Jacob, D.; Spurr, D.R.; Wang, J.; Shinozuka, Y.; Anderson, B.; Clarke, A.; Dibb, J.; McNaughton, C.; Weber, R. Synthesis of satellite (MODIS), aircraft (ICARTT), and surface (IMPROVE, EPA-AQS, AERONET) aerosol observations over eastern North America to improve MODIS aerosol retrievals and constrain surface aerosol concentrations and sources. *J. Geophys. Res. Atmos.* **2010**, *115*, doi:10.1029/2009JD012629.
41. Jones, T.A.; Christopher, S.A.; Quaas, J. A six year satellite-based assessment of the regional variations in aerosol indirect effects. *Atmos. Chem. Phys.* **2009**, *9*, 4091–4114.
42. Remer, L.A.; Kleidman, R.G.; Levy, R.C.; Kaufman, Y.J.; Tanre, D.; Mattoo, S.; Martins, J.V.; Ichoku, C.; Koren, I.; Yu, H.; *et al*. Global aerosol climatology from the MODIS satellite sensor. *J. Geophys. Res.* **2008**, *113*, doi:10.1029/2007JD009661.
43. Várnai, T.; Marshak, A. Analysis of co-located MODIS and CALIPSO observations near clouds. *Atmos. Meas. Tech. Discuss.* **2011**, *4*, 6861–6881.
44. Stockwell, W.R.; Kirchner, F.; Kuhn, M.; Seefeld, S. A new mechanism for regional atmospheric chemistry modeling. *J. Geophys. Res.* **1997**, *102*, 25847–25879.
45. Ackermann, I.J.; Hass, H.; Memmesheimer, M.; Ebel, A.; Binkowski, F.S.; Shankar, U. Modal aerosol dynamics model for Europe: Development and first applications. *Atmos. Environ.* **1998**, *32*, 2981–2999.
46. Wu, L.; Su, H.; Jiang, J.H. Regional simulations of deep convection and biomass burning over South America: 1. Model evaluations using multiple satellite data sets. *J. Geophys. Res.* **2011**, *116*, doi:10.1029/2011JD016105.

47. Fast, J.D.; Gustafson, W.I.; Chapman, E.G.; Easter, R.C.; Rishel, J.P.; Zaveri, R.A.; Grell, G.A.; Barth, M.C. The aerosol modeling testbed: A community tool to objectively evaluate aerosol process modules. *Bull. Am. Meteorol. Soc.* **2011**, *92*, 343–360.
48. Peckham, S.; Grell, G.; McKeen, S.; Barth, M.; Pfister, G.; Wiedinmyer, C.; Fast, J.; Gustafson, W.; Ghan, S.; Zaveri, R.; *et al*. WRF/Chem Version 3.3 User's Guide. In *NOAA*; NOAA Technical Memo.: Boulder, CO, USA, 2011; p. 98.
49. Choobari, O.A.; Zawar-Reza, P.; Sturman, A. Atmospheric forcing of the three-dimensional distribution of dust particles over Australia: A case study. *J. Geophys. Res.* **2012**, *117*, doi:10.1029/2012JD017748.
50. Grell, G.; Freitas, S.R.; Stuefer, M.; Fast, J. Inclusion of biomass burning in WRF-Chem: Impact of wildfires on weather forecasts. *Atmos. Chem. Phys.* **2011**, *11*, 5289–5303.
51. Barnard, J.C.; Fast, J.D.; Paredes-Miranda, G.; Arnott, W.P.; Laskin, A. Technical note: Evaluation of the WRF-Chem "Aerosol Chemical to Aerosol Optical Properties" module using data from the MILAGRO campaign. *Atmos. Chem. Phys.* **2010**, *10*, 7325–7340.
52. Saide, P.E.; Spak, S.N.; Carmichael, G.R.; Mena-Carrasco, M.A.; Howell, S.; Leon, D.C.; Snider, J.R.; Bandy, A.R.; Collett, J.L.; Benedict, K.B.; *et al*. Evaluating WRF-Chem aerosol indirect effects in Southeast Pacific marine stratocumulus during VOCALS-REx. *Atmos. Chem. Phys. Discuss.* **2011**, *11*, 29723–29775.
53. Jiang, F.; Liu, Q.; Huang, X.; Wang, T.; Zhuang, B.; Xie, M. Regional modeling of secondary organic aerosol over China using WRF/Chem. *J. Aerosol Sci.* **2012**, *43*, 57–73.
54. Schultz, M.G.; Backman, L.; Balkanski, Y.; Bjoerndalsaeter, S.; Brand, R.; Burrows, J.P.; Dalsoeren, S.; Vasconcelos, M.D.; Grodtmann, B.; Hauglustaine, D.A.; *et al. REanalysis of the TROpospheric Chemical Composition over the Past 40 years (RETRO)—A Long-Term Global Modeling Study of Tropospheric Chemistry Final Report*; Max Planck Institute for Meteorology, Hamburg: Jülich/Hamburg, Germany, 2007.
55. Olivier, J.G.J.; van Aardenne, J.A.; Dentener, F.J.; Pagliari, V.; Ganzeveld, L.N.; Peters, J.A.H.W. Recent trends in global greenhouse gas emissions: Regional trends 1970–2000 and spatial distributionof key sources in 2000. *Environ. Sci.* **2005**, *2*, 81–99.
56. Guenther, A.; Karl, T.; Harley, P.; Wiedinmyer, C.; Palmer, P.I.; Geron, C. Estimates of global terrestrial isoprene emissions using MEGAN (Model of Emissions of Gases and Aerosols from Nature). *Atmos. Chem. Phys.* **2006**, *6*, 3181–3210.
57. Menzel, W.P.; Frey, R.A.; Baum, B.A.; Zhang, H. *Cloud Top Properties and Cloud Phase Algorithm Theoretical Basis Document*; NASA: USA, 2006.
58. Geosciences-Australia, Global Map Australia 1M 2001 Product User Guide. In *Geosciences-Australia*; Australian Government: Canberra, Australia, 2004.
59. Radhi, M.; Box, M.A.; Box, G.P.; Mitchell, R.M.; Cohen, D.D.; Stelcer, E.; Keywood, M.D. Optical, physical and chemical characteristics of Australian continental aerosols: Results from a field experiment. *Atmos. Chem. Phys.* **2010**, *10*, 5925–5942.
60. Sorooshian, A.; Feingold, G.; Lebsock, M.D.; Jiang, H.; Stephens, G.L. Deconstructing the precipitation susceptibility construct: Improving methodology for aerosol-cloud precipitation studies. *J. Geophys. Res.* **2010**, *115*, doi:10.1029/2009JD013426.

61. Warneck, P.; Williams, J. *The Atmospheric Chemist's Companion, Numerical Data for Use in the Atmospheric Sciences*; Springer, 2012.
62. Dixon, P.G.; Mote, T.L. Patterns and causes of Atlanta's urban heat island–initiated precipitation. *J. Appl. Meteorol.* **2003**, *42*, 1273–1284.